catalysts

MDPI

Article

Well-Defined Ultrasmall V-NiP_2 Nanoparticles Anchored g-C_3N_4 Nanosheets as Highly Efficient Visible-Light-Driven Photocatalysts for H_2 Evolution

Mengfan Niu [1,2], Liyun Cao [1,2,*], Qianqian Liu [3], Xiaoyi Li [1,2], Qian Chen [1,2], Dinghan Liu [4], Wenbin Li [1], Jianfeng Huang [1,2,*] and Liangliang Feng [1,2,*]

1 Key Laboratory of Auxiliary Chemistry and Technology for Chemical Industry, Ministry of Education, Shaanxi University of Science and Technology, Xi'an 710021, China
2 School of Materials Science and Engineering, Shaanxi University of Science and Technology, Xi'an 710021, China
3 School of Materials Science and Engineering, Xi'an University of Science and Technology, Xi'an 710021, China
4 School of Electronic Information and Artificial Intelligence, Shaanxi University of Science and Technology, Xi'an 710021, China
* Correspondence: caoliyun@sust.edu.cn (L.C.); huangjf@sust.edu.cn (J.H.); fengll@sust.edu.cn (L.F.)

Abstract: Exploring low-cost and highly active, cost-effective cocatalysts is of great significance to improve the hydrogen evolution performance of semiconductor photocatalysts. Herein, a novel ultrasmall V-doped NiP_2 nanoparticle, as an efficient cocatalyst, is reported to largely upgrade the photocatalytic hydrogen evolution reaction (HER) of g-C_3N_4 nanosheets under visible-light irradiation. Experimental results demonstrate that V-NiP_2 cocatalyst can enhance the visible-light absorption ability, facilitate the separation of photo-generated electron-hole pairs and boost the transfer ability of electrons of g-C_3N_4. Moreover, the V-NiP_2/g-C_3N_4 hybrid exhibits prominent photocatalytic HER activity 17 times higher than the pristine g-C_3N_4 counterpart, even outperforming the 1 wt.% platinum-loaded g-C_3N_4. This work displays that noble-metal-free V-NiP_2 cocatalyst can serve as a promising and efficient alternative to Pt for high-efficiency photocatalytic H_2 evolution.

Keywords: g-C_3N_4; cocatalyst; V-NiP_2; photocatalyst; hydrogen evolution reaction

Citation: Niu, M.; Cao, L.; Liu, Q.; Li, X.; Chen, Q.; Liu, D.; Li, W.; Huang, J.; Feng, L. Well-Defined Ultrasmall V-NiP_2 Nanoparticles Anchored g-C_3N_4 Nanosheets as Highly Efficient Visible-Light-Driven Photocatalysts for H_2 Evolution. *Catalysts* **2022**, *12*, 998. https://doi.org/10.3390/catal12090998

Academic Editors: Shiva Mohajernia, Manuela S. Killian and Anca Mazare

Received: 30 July 2022
Accepted: 1 September 2022
Published: 5 September 2022

1. Introduction

The excessive dependence on non-renewable fossil fuels has largely promoted the research on sustainable clean energy [1–3]. Hydrogen energy is widely regarded as an ideal green fuel alternative to fossil ones, and thus it is highly urgent and significant to find an effective, environmentally friendly approach to producing H_2 [4–7]. Photocatalytic water splitting holds great promise in terms of clean, large-scale and sustainable hydrogen production, whose hydrogen evolution efficiency extremely depends on the catalytic properties of photocatalysts [8–11]. In order to capture and utilize the visible light that dominates in the solar energy spectrum, it is quite imperative to explore the highly active and stable visible-light-driven photocatalysts for hydrogen evolution reaction (HER).

At present, a large number of photocatalysts are applied to hydrogen production from water under visible light. Graphitic carbon nitride (g-C_3N_4), a promising metal-free semiconducting polymer, has been given widespread attention in the realm of photocatalytic water splitting, photodegradation of pollutants and photocatalytic reduction in CO_2 due to its advantages of being environmentally benign and low cost, with excellent chemical stability and a suitable band gap of about 2.7 eV [12–15]. However, the insufficient light absorption and rapid recombination of photo-generated electron-hole pairs have restricted the photocatalytic activity of pure g-C_3N_4 [11,16]. In recent years, researchers have made a lot of effort to improve the activity of g-C_3N_4, such as controlling its structure and morphology, coupling with other cocatalysts, and constructing the heterostructure [17–21]. Noble

metal Pt is a brilliant cocatalyst of g-C_3N_4, but its scarce reserves and exorbitant price greatly hamper its practice applications [22,23]. In order to improve the photocatalytic HER performance of g-C_3N_4 under visible light, it has been an urgent task to develop cheap, efficient cocatalysts. It is reported that transition metal phosphide (TMP) catalysts are considered promising to replace precious metal-based cocatalysts to improve photocatalytic HER efficiency [24–28]. Thereinto, NiP_2 possesses the characteristics of good electrical conductivity, corrosion resistance and stable chemical structure so that it can be applied as an electrode material for a metal ion battery and electrocatalysis [29–31]. Most recently, NiP_2 as a cocatalyst has attracted a lot of attention in relation to photocatalytic hydrogen evolution. For example, Yan et al. reported a novel NiP_2/Cu_3P p-n heterojunction cocatalyst for improving the photocatalytic hydrogen evolution of g-C_3N_4; this material has good HER activity but unsatisfactory stability [32]. Yang et al. designed a novel NiP_2/g-C_3N_4 heterojunction via a homogeneous precipitation method assisted by a thermal phosphorization reaction, in which NiP_2 nanoparticles agglomerated severely, resulting in weak light absorption [33]. Thus, the incorporation of ultrasmall NiP_2 nanoparticles into g-C_3N_4 for boosted photocatalytic HER performance is worthy of consideration. In addition, metal (Mn, Cr, V) doping is confirmed to be an effective route to improve the catalytic HER performance of semiconductors [34–36]. For instance, V-doped MoS_2 material presented good HER activity because the V-doping is conducive to optimizing the electronic structure, increasing the active site, and accelerating the electronic transfer process of the pristine MoS_2 [37]. Therefore, it is highly valuable to explore whether V-NiP_2 can be an effective cocatalyst of g-C_3N_4 for photocatalytic HER.

In this work, V-NiP_2 was reported, for the first time, as a cocatalyst of g-C_3N_4, and the as-synthesized V-NiP_2/g-C_3N_4 material showed prominent photocatalytic HER under visible light ($\geq$420 nm), even outperforming the 1 wt.% Pt-loaded g-C_3N_4. Such excellent photocatalytic activity of V-NiP_2/g-C_3N_4 is mainly attributed to the enhanced absorption capability of visible light, fast electron transfer rate, and the depressed recombination of photogenerated electron-hole pairs, as well as abundant catalytic sites over the V-NiP_2-loading g-C_3N_4 nanosheets.

2. Results and Discussion

The X-ray diffraction (XRD) patterns in Figure 1a are utilized to identify the crystal structure of pure g-C_3N_4 and V-NiP_2/g-C_3N_4. As shown in Figure 1a, for the pure g-C_3N_4, two strong XRD diffraction peaks at 13.1° and 27.8° correspond to the (100) plane of the in-plane structural packing motif of tristriazine and the (200) plane of the interlayer stacking with aromatic systems, respectively (PDF#87-1526) [38–40]. In addition, some obvious diffraction peaks at 28.34°, 32.85°, 36.86°, 40.52, 47.14°, 55.92°, 58.64°, 61.25°, 63.87°, 76.08° and 78.43°, which are matched well with the (111), (200), (210), (211), (220), (311), (222), (320), (321) and (331) planes of NiP_2 (JCPDS#21-0590), respectively [41]. The results indicate that the V-Ni_2P/G-C_3N_4 composite is successfully prepared through the phosphating-calcination process. Figure 1b–d and Figure S1 record the surface chemical states of C, N, V, Ni and P for V-NiP_2/g-C_3N_4 by using X-ray photoelectron spectroscopy (XPS). The C 1s spectra are shown in Figure S1a, three obvious deconvolution peaks at 284.6 eV, 286.02 eV and 288.25 eV can be observed, which correspond to the C–C and C–NH_2 group, and the sp^2-hybridized N–C=N in the aromatic ring, respectively [42]. The supreme deconvolution peaks of N 1 s in Figure S1b at 398.2 eV are assigned to the C–N=C structure from g-C_3N_4, the other peaks at 398.2 eV, 398.9 eV, 400.5 eV and 404.1 eV are attributed to C–N=C, N–$(C)_3$, C–N–H and π excitations of the C=N conjugated structures in g-C_3N_4 [43]. Figure 1b demonstrates the presence of V, which has two deconvolution peaks at 516.9 eV for the V $2p_{3/2}$ and 524.4 eV for V $2p_{1/2}$ ascribed to the V–P bond [44]. As shown in Figure 1c, two peaks of Ni $2p_{3/2}$ (856.4 eV) and Ni $2p_{1/2}$ (874.4 eV) for V-NiP_2/g-C_3N_4 can be attributed to Ni^{2+}; the peaks at 862.6 eV and 880.6 eV correspond to Ni $2p_{3/2}$ and Ni $2p_{1/2}$, respectively [45], and the Ni-P binding energy is located at 853.7 eV [46]. For the P

2p XPS spectrum in Figure 1d, the peak appearing at 130 eV is attributed to the Ni-P bond, while the peak at 133.6 eV is due to the inevitable surface oxidation of P [47].

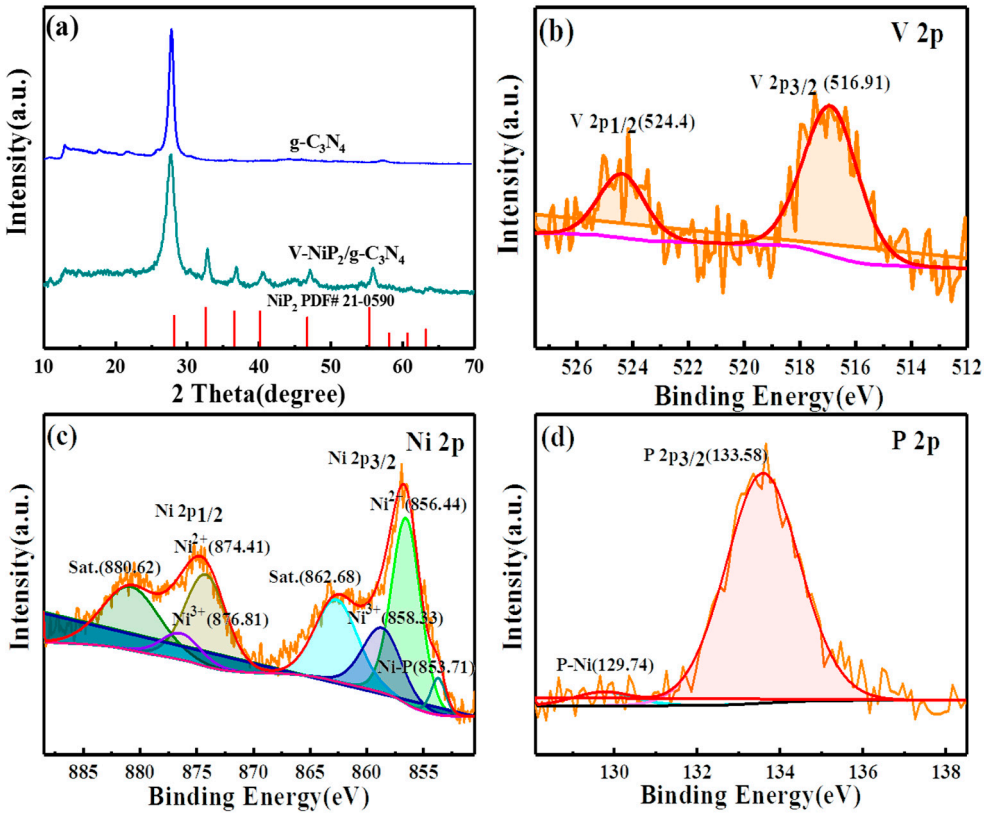

Figure 1. (**a**) XRD patterns of g-C_3N_4 and V-NiP_2/g-C_3N_4; The XPS spectra of (**b**) V 2p. (**c**) Ni 2p, and (**d**) P 2p for V-NiP_2/g-C_3N_4.

The SEM images in Figure S2a,b show the morphology and microstructure of g-C_3N_4 and V-NiP_2/g-C_3N_4 samples. Pure g-C_3N_4 presents an irregular bulk morphology stacked by nanosheets in Figure S2a. While V-NiP_2/g-C_3N_4 displays the crossed nanosheet structure attached with nanoparticles.

We further characterize the microstructure of the V-NiP_2/g-C_3N_4, as shown in Figure 2. As shown in Figure 2a, it can be observed that a large number of nanoparticles grow on the nanosheets. As shown in Figure 2b, we have an in-depth observation of the nanoparticles, and it can be seen that the obvious lattice spacing of 0.27nm corresponds to the (200) interplanar spacing of cubic NiP_2 (PDF#21-0590) [30]. To obtain the size distribution of the V-NiP_2 cocatalyst, some more HRTEM images of V-NiP_2/g-C_3N_4 photocatalyst were made (Figure S3), and the size of V-NiP_2 nanoparticles was not considerably uniform and was examined to 3–8 nm due to the employed solid calcination method. The elemental mapping of V-NiP_2/g-C_3N_4 is presented in Figure 2e, and C, N, Ni, V and P elements are uniformly distributed in the whole photocatalyst, illustrating that the V-Ni_2P nanoparticles are dispersedly loaded on the surface of the g-C_3N_4 nanosheet surface. All these characterizations strongly indicate that the NiV-LDH precursor was successfully converted into V-NiP_2 via a phosphorization reaction.

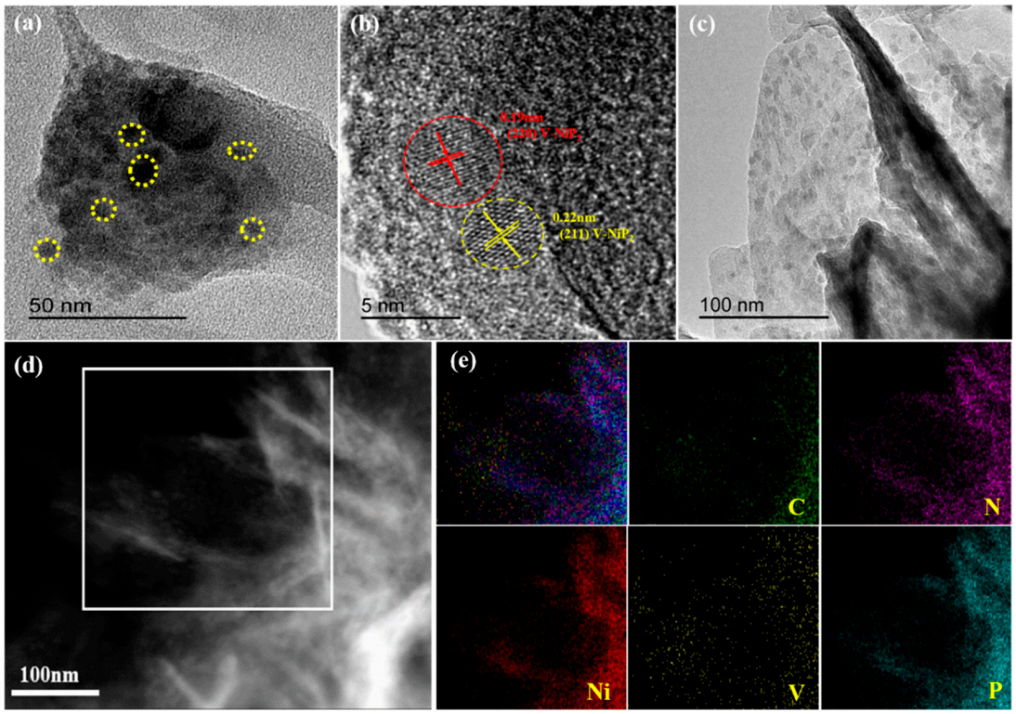

Figure 2. (**a**,**c**) TEM of V-NiP_2/g-C_3N_4, (**b**) HRTEM of V-NiP_2/g-C_3N_4; (**d**,**e**) elemental mapping of C, N, Ni, V, and P, respectively.

In order to determine the photocatalytic hydrogen evolution activity of all samples, photocatalytic tests were carried out with triethanolamine acid (TEOA) as a sacrificial agent under a 300 W lamp irradiation for 4 h. As presented in Figure 3a, pure g-C_3N_4 shows trace hydrogen evolution amounts due to the fast photogenerated carrier recombination and low-light absorption capacity [48]. However, V-NiP_2/g-C_3N_4 composites present an obvious improved HER performance with a hydrogen production rate of 1426.82 μmol g^{-1}, even higher than the 1%wt Pt/g-C_3N_4 (1116 μmol g^{-1}). Furthermore, the as-prepared V-NiP_2/g-C_3N_4 material exhibits much higher than most of the other g-C_3N_4-based photocatalysts (Table S1) [23,26,27,30,36–39]. The excellent catalytic HER activity can be mainly ascribed to the following three aspects: (i) the facilitated absorption of the visible-light region of g-C_3N_4 due to the incorporation of black V-NiP_2 nanoparticles; (ii) the enhanced electron transfer rate resulting from the good electrical conductivity of V-NiP_2; and (iii) the inhibited recombination rate of photogenerated electron-hole pairs on the g-C_3N_4 photocatalyst because the V-NiP_2, as the electron trapping agent, can capture the photo-generated electron quickly. To evaluate the long-term stability of V-NiP_2/g-C_3N_4, five cycles of H_2 production experiments are shown in Figure 3b, no distinct decrease in the hydrogen evolution amount is observed, illustrating that V-NiP_2/g-C_3N_4 maintains good stability. In order to verify the structure's stability, the microstructure of V-NiP_2/g-C_3N_4 after the test is characterized by HRTEM and elemental mapping, as shown in Figure S5. It can be seen that the NiP_2 phase still exists in the used photocatalysts, and C, N, P, V and Ni elements are distributed in this material, indicating its structural stability during 20 h photocatalytic HER.

The light capture properties of pure g-C_3N_4 and V-NiP_2/g-C_3N_4 samples were analyzed by the UV–vis diffuse reflection measurement. In Figure 4a, the pure g-C_3N_4 has weak absorption of visible light, but its absorption intensity gradually increases as the wavelength decreases from visible light to ultraviolet light, and its absorption edge is around 470 nm. As shown in Figure S4, the calculated pure g-C_3N_4 band gap is ~2.78 eV, which is consistent with the theoretical value of g-C_3N_4. The V-NiP_2/g-C_3N_4 sample presents a considerably improved absorption in the UV–vis light region compared with pure g-C_3N_4, indicating that V-NiP_2 is able to help g-C_3N_4 harvest more visible light [49]. As for V-NiP_2/g-C_3N_4, the corresponding band gap is calculated to be 2.75 eV, as shown

in Figure S3, and there is no obvious change compared with pure g-C_3N_4, implying that V-NiP_2 did not dope into the g-C_3N_4 crystal lattice to change its band gap. This phenomenon indicates that V-NiP_2 as a g-C_3N_4 cocatalyst, effectively promotes the visible-light absorption capacity of the V-NiP_2/g-C_3N_4 photocatalyst.

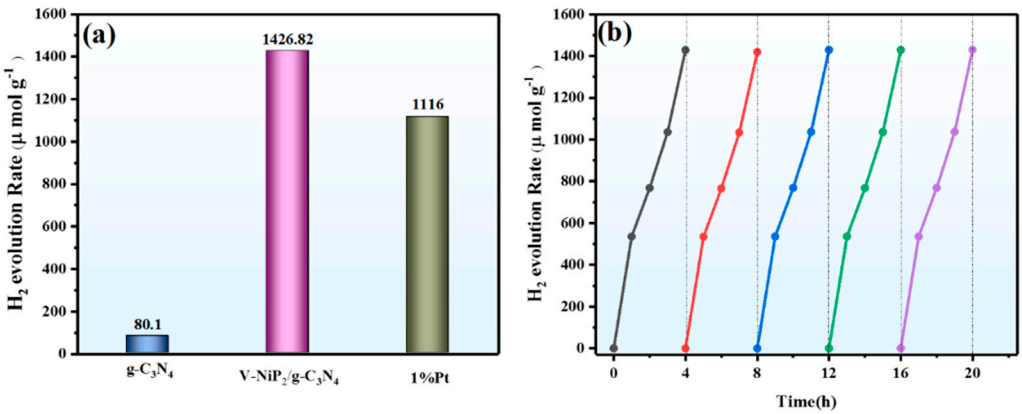

Figure 3. (**a**) Photocatalytic H_2 evolution rate of g-C_3N_4, V-NiP_2/g-C_3N_4 and 1%wt Pt/g-C_3N_4; (**b**) The cycling stability experiments of photocatalytic H_2 evolution for V-NiP_2/g-C_3N_4 under visible light irradiation for 20 h.

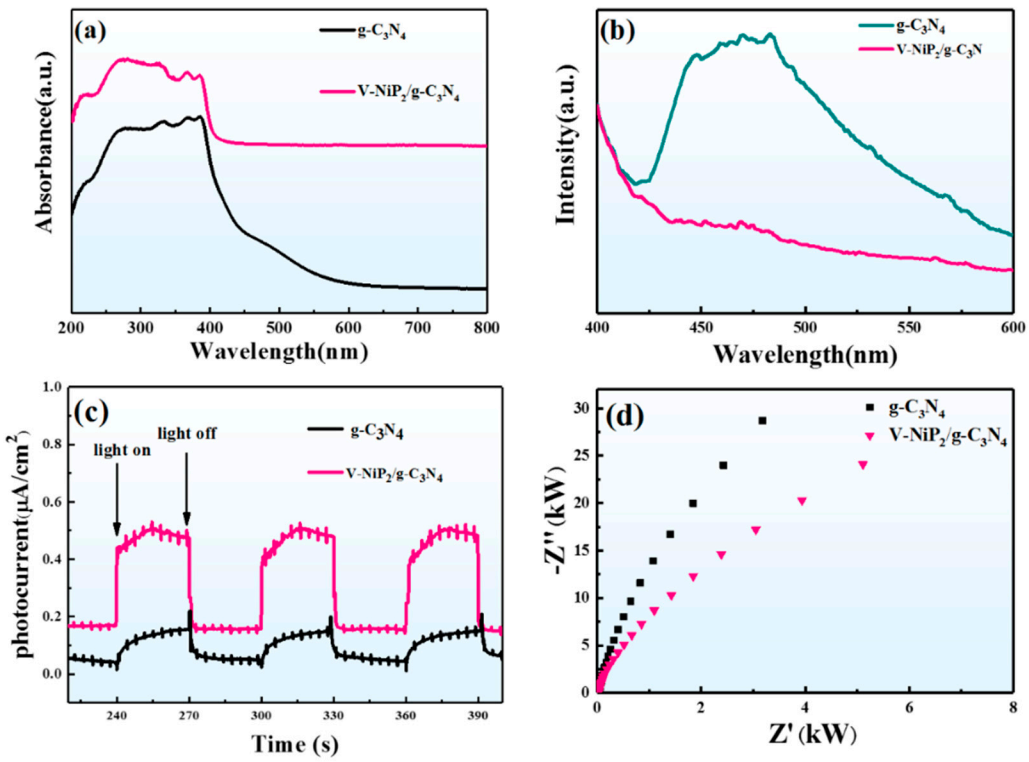

Figure 4. (**a**) UV–vis diffuse reflection spectra of pure g-C_3N_4 and V-NiP_2/g-C_3N_4; (**b**) The photoluminescence (PL) spectra of g-C_3N_4 and V-NiP_2/g-C_3N_4; (**c**) Transient photocurrent responses of g-C_3N_4 V-NiP_2/g-C_3N_4; (**d**) EIS Nyquist plots of g-C_3N_4 and V-NiP_2/g-C_3N_4 in 0.5M Na_2SO_4 solution visible light irradiation.

In order to verify the interfacial charge separation of V-NiP_2/g-C_3N_4, Figure 4b displays the photoluminescence spectra of g-C_3N_4 and V-NiP_2/g-C_3N_4 samples. Under the examination wavelength of 363 nm, g-C_3N_4 exhibits an emission peak at 483nm. The PL intensity of V-NiP_2/g-C_3N_4 is obviously lower than that of pure g-C_3N_4. To reveal

the transfer and separation of the photogenerated electron-hole pairs, the transient photocurrent density vs. time curves are carried out at the turn on or off the light condition. Pristine g-C_3N_4 and V-NiP_2/g-C_3N_4 are coated on FTO glass, respectively, as working electrodes to dry for 24 h in the air, measured in a mixed solution of 0.5 M Na_2SO_4 solution under discontinuous visible-light irradiation. The pure g-C_3N_4 shows a weak photocurrent response at each on-off light irradiation compared to V-NiP_2/g-C_3N_4; the notably increased photocurrent intensity of the V-NiP_2/g-C_3N_4 phenomenon demonstrates that V-NiP_2 is effective in preventing the combination of the photogenerated electron-hole pairs, which is consistent with the prolonged photogenerated charges lifetime. The electrochemical impedance spectroscopy (EIS) Nyquist plots in Figure 4d show that V-NiP_2/g-C_3N_4 displays a much smaller semicircle diameter compared to g-C_3N_4, illustrating the smaller charge transfer resistance, which contributes to the fast transfer of the photo-generated electron to the surface of V-NiP_2/g-C_3N_4 for the improved HER.

Through discussion and analysis of the above experiment results, a plausible photocatalytic mechanism schematic in Figure 5 is carried out to help understand the specific photocatalytic hydrogen evolution reaction process of the V-NiP_2/g-C_3N_4 photocatalyst. Under visible-light irradiation, the electrons of g-C_3N_4 on the valence band (VB) absorb the energy of photons, and then become excited and are transferred to the conduction band (CB), owing to the metallic character of V-NiP_2. The photogenerated electrons are trapped by the V-NiP_2 and easily and rapidly migrate to the V-NiP_2 passing through the intimate interface, so the combination of photogenerated electron-hole pairs is retarded. Subsequently, the photo-generated electrons on the surface of V-NiP_2 combine with H^+ ions to form H_2 molecules and are released from the water. Simultaneously, the photo-generated holes on the valence band of g-C_3N_4 will be timely depleted by the TEOA sacrificial reagent. Therefore, the photocatalytic hydrogen performance is greatly improved with the help of the V-NiP_2 cocatalyst.

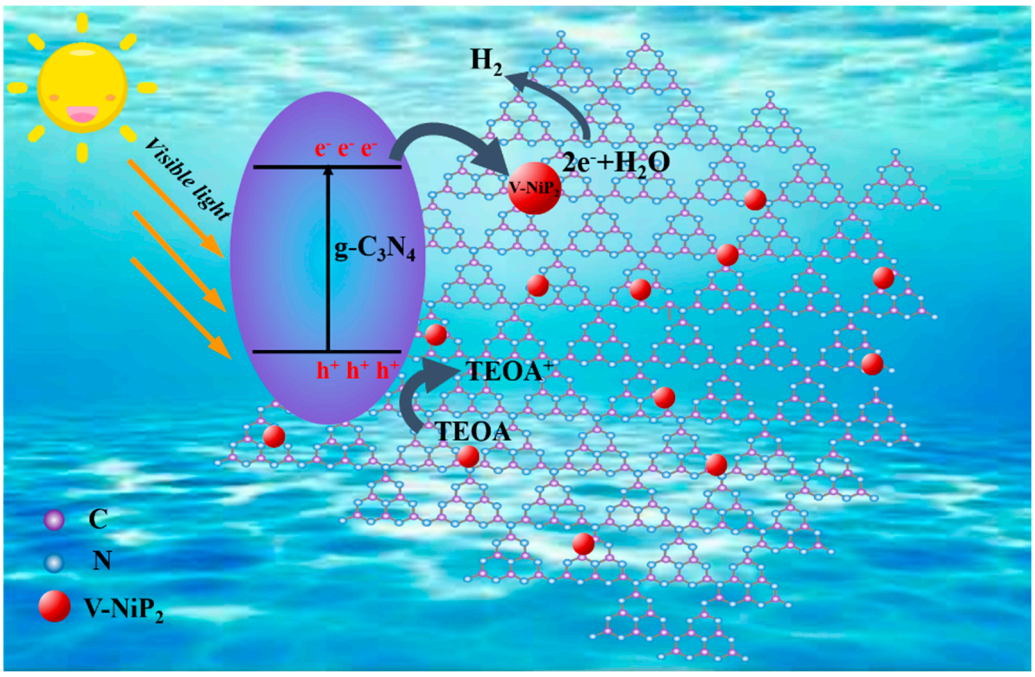

Figure 5. Photocatalytic mechanism schematic of V-NiP_2/g-C_3N_4 photocatalyst for H_2 evolution under visible-light irradiation.

3. Materials and Methods

3.1. Chemicals and Materials

Melamine was purchased from Tianjin Kermel Chemical Co., Ltd. Nickel (II) chloride hexahydrate ($NiCl_2 \cdot 6H_2O$), vanadium chloride (III) (VCl_3, ≥97%), Urea (CH_4N_2O, ≥98%),

ammonium fluoride (NH_4F, ≥96%) and ethanol absolute (CH_3CH_2OH, ≥99.8%) were purchased from Sinopharm Chemical Reagent Co., Ltd., (Shanghai, China). Sodium hypophosphite (NaH_2PO_2, ≥99%) and chloroplatinic acid hexahydrated ($H_2PtCl_6 \cdot 6H_2O$, ≥37%) were purchased from Aladdin Reagent Co., Ltd., (Shanghai, China). Triethanolamine ($N(CH_2CH_2OH)_3$, ≥98%) was purchased from Tianli Chemical Reagent Co, Ltd., (Tianjin, China). All chemicals are analytical grade and used without further purification.

3.2. Synthesis of the V-NiP_2/g-C_3N_4 Composite

3.2.1. Synthesis of Bulk g-C_3N_4

Bulk g-C_3N_4 was synthesized by calcining melamine in a muffle furnace with the temperature kept at 550 °C for 4 h with a heating rate of 5 °C min^{-1}. After cooling down to room temperature, the yellow product of g-C_3N_4 was ground into power in an agate mortar for further use.

3.2.2. Synthesis of the NiV-LDH/g-C_3N_4 Precursor

The NiV-LDH/g-C_3N_4 precursor was prepared by a hydrothermal method. Specifically, 0.475 g of $NiCl_2 \cdot 6H_2O$, 0.063 g of VCl_3, 1 g of Urea and 0.24 g of NH_4F were put into a clean beaker with 40 mL of deionized water, then 3 g of g-C_3N_4 was added into the beaker and stirred for 30 min. Then, it was transferred into a Teflon-lined Autoclave, maintained at 120 °C for 16 h. After cooling down to room temperature, the depositions were separated and washed with deionized water and absolute ethanol three times, separately. The obtained products were dried in an oven at 60 °C overnight, following which we obtained the 7.8%wt NiV-LDH/g-C_3N_4 precursor.

3.2.3. Synthesis of V-NiP_2/g-C_3N_4 Composite

Firstly, 2 g of NaH_2PO_2 was placed upstream of a big porcelain boat, and 200 mg of prepared 7.8%wt NiV-LDH/g-C_3N_4 precursor was put downstream of the big porcelain boat, then transferred into a tube furnace and calcined in the Ar gas atmosphere at 500 °C for 2 h with a heating rate of 5 °C min^{-1}.

3.3. Characterizations

The crystal phases of the materials were examined by Rigaku, D/max-2200pc X-ray diffractometer (XRD) with Cu Kα irradiation at a scanning rate of 8° min^{-1}. The morphology and microstructures were investigated using field emission scanning electron microscopy (Hitachi, S4800) and transmission electron microscopy (Tecnai G2 F20S-TWIN), respectively. The surface elemental composition and chemical state were analyzed by X-ray photoelectron spectroscopy (XPS) of a Surface Science Instruments Spectrometer with monochromatic Al Kα source. The Ultraviolet–visible (UV-vis) absorption spectra were obtained on Cary 5000 UV–vis spectrometer (Agilent). The photoluminescence (PL) spectra and time-resolved photoluminescence decay spectra were measured on Edinburgh FS5 spectrophotometer.

3.4. Photocatalytic Hydrogen Evolution Measurements

The photocatalytic hydrogen generation performance of the as-prepared V-NiP_2/g-C_3N_4 was evaluated by an automatic online photocatalytic test system (Labsolar-6A, Beijing Perfectlight Co., Ltd., Beijing, China). An amount of 50 mg of photocatalyst was firstly dispersed with strong stirring for 0.5 h in the 80 mL of slurry solution containing 15 mL of triethanolamine (TEOA, 15 vol%) at room temperature. Before the photocatalytic experiment, the slurry was transferred into a quartz flask and then a continuous magnetic stirrer was applied. Before light irradiation, the Labsolar-6A reaction system was bubbled with N_2 to remove the air. Using Agilent gas chromatography (GC-7890B, America) with N_2 as the carrier gas and TCD (Thermal Conductivity Detector) as the detector.

3.5. Photoelectrochemical Measurements

Transient photocurrent response and electrochemical impedance spectroscopy (EIS) measurements were performed on an electrochemical workstation (CHI 660E, Shanghai Chenhua Instruments, Shanghai, China) using three standard electrodes with Pt wire, $Hg/HgCl_2$ and 0.5 M Na_2SO_4 solution as a reference electrode, counter electrode and electrolyte, respectively. The working electrode was prepared on a clean FTO glass (2 cm × 2 cm). Specifically, 10 mg of photocatalyst was dispersed in 150 μL of isopropanol and 10 μL of Nafion solution, followed by sonication for 30 min. Finally, the slurry was homogenized, coated on FTO glass, and dried naturally for 24 h. The visible-light source was a 300 W Xe lamp (PLS-SXE 300 D, Beijing Perfect Light Technology Co., Ltd., Beijing, China) with a UV-cut filter ($\lambda \geq 420$ nm).

4. Conclusions

In conclusion, a novel well-defined ultra-small V-NiP_2 nanoparticle was successfully developed as an effective cocatalyst of g-C_3N_4 to improve photocatalytic HER activity under visible-light irradiation (≥420 nm). Benefitting from the enhanced visible-light absorption ability, the separation of photo-generated carriers was facilitated, the recombination of photogenerated electron-hole pairs was weakened, and the electron transfer ability was boosted, with the resulting V-NiP_2/g-C_3N_4 hybrid exhibiting prominent photocatalytic HER activity 17 times higher than the pristine g-C_3N_4 counterpart, even outperforming the 1 wt.% platinum-loaded g-C_3N_4. Our work shown here injects new impetus to develop transition metal phosphides as low-cost and high-performance cocatalysts of g-C_3N_4 for efficient photocatalytic HER.

Supplementary Materials: The following supporting information can be downloaded at: https://www.mdpi.com/article/10.3390/catal12090998/s1, Figure S1: The XPS spectra of (a) C 1s, (b) N 1s for V-NiP_2/g-C_3N_4; Figure S2: SEM of (a) g-C_3N_4, (b) V-NiP_2/g-C_3N_4; Figure S3: HRTEM of V-NiP_2/g-C_3N_4; Figure S4:The banding energy of pure g-C3N4 and V-NiP_2/g-C_3N_4; Figure S5: HRTEM and elemental mapping of V-NiP_2/g-C_3N_4 after test; Table S1: Summary of the Photocatalytic H_2 Evolution on g-C_3N_4-Based Photocatalysts.

Author Contributions: Conceptualization, L.C. and J.H.; Data curation, M.N.; Formal analysis, Q.L. and L.F.; Investigation, M.N., X.L., W.L. and Q.C. Methodology, L.C., L.F. and D.L. Supervision, L.C.; L.F. and J.H. Writing—original draft preparation, M.N.; Writing—review and editing, M.N. and Q.L. All authors have read and agreed to the published version of the manuscript.

Funding: This work was supported by the National Natural Science Foundation of China (Nos. 22179074, 52073166), Natural Science Basic Research Program of Shaanxi (Program No. 2022JQ-481), the Xi'an Key Laboratory of Green Manufacture of Ceramic Materials Foundation (No. 2019220214-SYS017CG039), the Key Program for International S&T Cooperation Projects of Shaanxi Province (2020KW-038, 2020GHJD-04), Science and Technology Program of Xi'an, China (2020KJRC0009), Science and Technology Resource Sharing Platform of Shaanxi Province (2020PT-022), Science and Technology Plan of Weiyang District, Xi'an (202009), Open foundation of Key Laboratory of Auxiliary Chemistry and Technology for Chemical Industry, Ministry of Education (KFKT2020-01).

Conflicts of Interest: The authors declare no conflict of interest.

References

1. Chu, S.; Majumdar, A. Opportunities and challenges for a sustainable energy future. *Nature* **2012**, *488*, 294. [CrossRef] [PubMed]
2. Liao, G.; Gong, Y.; Zhang, L.; Gao, H.; Yang, G.; Fang, B. Semiconductor polymeric graphitic carbon nitride photocatalysts: The "holy grail" for the photocatalytic hydrogen evolution reaction under visible light. *Energy Environ. Sci.* **2019**, *12*, 2080–2147. [CrossRef]
3. Wang, W.; Bai, X.; Ci, Q.; Du, L.; Ren, X.; Phillips, D. Near-Field Drives Long-Lived Shallow Trapping of Polymeric C3N4 for Efficient Photocatalytic Hydrogen Evolution. *Adv. Funct. Mater.* **2021**, *31*, 795–802. [CrossRef]
4. Shao, Z.; Meng, X.; Lai, H.; Zhang, D.; Pu, X.; Su, C.; Li, H.; Ren, X.; Geng, Y. Coralline-like Ni_2P decorated novel tetrapod-bundle $Cd_{0.9}Zn_{0.1}S$ ZB/WZ homojunctions for highly efficient visible-light photocatalytic hydrogen evolution. *Chin. J. Catal.* **2021**, *42*, 439–449. [CrossRef]

5. Zhang, Y.; Cao, X.; Cao, Z. Unraveling the Catalytic Performance of the Nonprecious Metal Single-Atom-Embedded Graphitic s-Triazine-Based C_3N_4 for CO_2 Hydrogenation. *ACS Appl. Mater. Inter.* **2022**, *14*, 35844–35853. [CrossRef] [PubMed]
6. Zhu, Q.; Qiu, B.; Du, M.; Ji, J.; Muhammad Nasir, M. Xing, J. Zhang. Dopant-Induced Edge and Basal Plane Catalytic Sites on Ultrathin C3N4 Nanosheets for Photocatalytic Water Reduction. *ACS Sustain. Chem. Eng.* **2020**, *8*, 7497–7502. [CrossRef]
7. Liu, E.; Chen, J.; Ma, Y.; Feng, J.; Jia, J.; Fan, J.; Hu, X. Fabrication of 2D SnS_2/g-C_3N_4 heterojunction with enhanced H_2 evolution during photocatalytic water splitting. *J. Colliod Interf. Sci.* **2018**, *524*, 313–324. [CrossRef]
8. Wang, X.; Wang, F.; Sang, Y.; Liu, H. Full-Spectrum Solar-Light-Activated Photocatalysts for Light Chemical Energy Conversion. *Adv. Energy Mater.* **2017**, *7*, 1700473–1700488. [CrossRef]
9. Zou, Q.; Feng, K.; Zhong, J.; Mai, Y.; Zhou, Y. Single-Metal-Atom Polymeric Unimolecular Micelles for Switchable Photocatalytic H_2 Evolution. *CCS Chem.* **2020**, *2*, 1963–1971. [CrossRef]
10. Zhao, H.; Zhang, H.; Cui, G.; Dong, Y.; Wang, G.; Jiang, P.; Wu, X.; Zhao, N. A photochemical synthesis route to typical transition metal sulfides as highly efficient cocatalyst for hydrogen evolution: From the case of NiS/g-C_3N_4. *Appl. Catal. B-Environ.* **2018**, *225*, 284–290. [CrossRef]
11. Chen, M.; Guo, C.; Hou, S.; Lv, J.; Zhang, Y.; Zhang, H.; Xu, J. A novel Z-scheme AgBr/P-g-C_3N_4 heterojunction photocatalyst: Excellent photocatalytic performance and photocatalytic mechanism for ephedrine degradation. *Appl. Catal. B-Environ.* **2020**, *266*, 118614. [CrossRef]
12. Ran, J.; Ma, T.; Guo, G.; Du, X.; Qiao, S. Porous P-doped graphitic carbon nitride nanosheets for synergistically enhanced visible-light photocatalytic H_2 production. *Energy Environ. Sci.* **2015**, *8*, 3708–3717. [CrossRef]
13. Wang, X.; Maeda, K.; Thomas, A.; Takanabe, K.; Xin, G.; Carlsson, J.; Domen, K.; Antonietti, M. A metal-free polymeric photocatalyst for hydrogen production from water under visible light. *Nat. Mater.* **2009**, *8*, 76–80. [CrossRef] [PubMed]
14. Wu, M.; Yan, J.; Zhang, X.; Zhao, M.; Jiang, Q. Ag_2O modified g-C_3N_4 for highly efficient photocatalytic hydrogen generation under visible light irradiation. *J. Mater. Chem. A* **2015**, *3*, 15710–15714. [CrossRef]
15. Xue, W.; Hu, X.; Liu, E.; Fan, J. Novel reduced graphene oxidesupported $Cd_{0.5}Zn_{0.5}S$/g-C_3N_4 Z-scheme heterojunction photocatalyst for enhanced hydrogen evolution. *Appl. Surf. Sci.* **2018**, *447*, 783–794. [CrossRef]
16. Zhou, W.; Jia, T.; Zhang, D.; Zheng, Z.; Hong, W.; Chen, X. The enhanced cocatalyst free photocatalytic hydrogen evolution and stability based on indenofluorene-containing donor-acceptor conjugated polymer dots/g-C_3N_4 nanosheets heterojunction. *Appl. Catal. B-Environ.* **2019**, *259*, 118067. [CrossRef]
17. Ye, S.; Wang, R.; Wu, M. A review on g-C_3N_4 for photocatalytic water splitting and CO_2 reduction. *Appl. Surf. Sci.* **2015**, *358*, 15–27. [CrossRef]
18. Zheng, Y.; Lin, L.; Wang, B. Graphitic carbon nitride polymers toward sustainable photoredox catalysis. *Angew. Chem. Inter. Ed.* **2015**, *54*, 12868–12884. [CrossRef]
19. Kong, L.; Dong, Y.; Jiang, P.; Wang, G.; Zhang, H. Light-assisted rapid preparation of a Ni/g-C_3N_4 magnetic composite for robust photocatalytic H_2 evolution from water. *J. Mater. Chem. A* **2016**, *4*, 9998–10007. [CrossRef]
20. Zhao, H.; Dong, Y.; Jiang, P. In situ light-assis-ted preparation of MoS_2 on graphitic C_3N_4 nanosheets for enhanced photocatalytic H_2 production from water. *J. Mater. Chem. A* **2015**, *14*, 7375–7381. [CrossRef]
21. Dong, Y.; Kong, L.; Wang, G.; Jiang, P.; Zhao, N.; Zhang, H. Photochemical synthe-sis of Co_xP as cocatalyst for boosting photocatalytic H_2 production via spatial charge separation. *Appl. Catal. B Environ.* **2017**, *211*, 245–251. [CrossRef]
22. Tian, L.; Min, S.; Wang, F.; Zhang, Z. Metallic vanadium nitride as a noble-metal-free cocatalyst efficiently catalyze photocatalytic hydrogen production with CdS nanoparticles under visible light irradiation. *J. Phys. Chem. C* **2019**, *123*, 28640–28650. [CrossRef]
23. Shen, R.; Xie, J.; Zhang, H.; Zhang, A.; Chen, X.; Li, X. Enhanced solar fuel H_2 generation over g-C_3N_4 nanosheet photocatalysts by the synergetic effect of noble metal-free Co_2P cocatalyst and the environmental phosphorylation strategy. *ACS Sustain. Chem. Eng.* **2017**, *6*, 816–826. [CrossRef]
24. Dong, H.; Hong, S.; Zou, Y.; Zhang, X.; Lu, Z.; Han, J.; Wang, L.; Ni, L.; Li, C.; Wang, Y. Fabrication of 2D/0D Heterojunction Based on the Dual Controls of Micro/Nano-Morphology and Structure Towards High-Efficiency Photocatalytic H_2 Production. *ChemCatChem* **2019**, *11*, 5651–5660. [CrossRef]
25. Pi, M.; Zhang, D.; Wang, S.; Chen, S. Enhancing electrocatalytic hydrogen evolution of WP2 three-dimensional nanowire arrays via mo doping—Sciencedirect. *Mater. Lett.* **2018**, *213*, 315–318. [CrossRef]
26. Zeng, D.; Zhou, T.; Ong, W.; Mingda, W.; Duan, X.; Xu, W.; Chen, Y.; Zhu, Y. Sub-5 nm ultra-fine FeP nanodots as efficient co-catalysts modified porous g-C_3N_4 for precious-metal-free photocatalytic hydrogen evolution under visible light. *ACS Appl. Mater. Interfaces* **2019**, *11*, 5651–5660. [CrossRef] [PubMed]
27. Liu, W.; Shen, J.; Liu, Q.Q.; Yang, X.F.; Tang, H. Porous MoP network structure as co-catalyst for H_2 evolution over g-C_3N_4 nanosheets. *Appl. Surf. Sci.* **2018**, *462*, 822–830. [CrossRef]
28. Yue, X.Z.; Yi, S.S.; Wang, R.W.; Zhang, Z.T.; Qiu, S.L. A novel and highly efficient earth-abundant Cu_3P with TiO_2 "P-N" heterojunction nanophotocatalyst for hydrogen evolution from water. *Nanoscale* **2016**, *8*, 17516–17523. [CrossRef]
29. Alshorifi, T.; Alswat, A.; Mannaa, A.; Alotaibi, T.; El-Bahy, M.; Salama, S. Facile and Green Synthesis of Silver Quantum Dots Immobilized onto a Polymeric CTS–PEO Blend for the Photocatalytic Degradation ofFacile and Green Synthesis of Silver Quantum Dots Immobilized onto a Polymeric CTS–PEO Blend for the Photocatalytic Degradation of p-Nitrophenol. *ACS Omega* **2022**, *6*, 30432–30441. [CrossRef]

30. Mannaa, A.; Qasim, F.; Alshorifi, T.; I-Bahy, M.E.; Salama, S. Role of NiO Nanoparticles in Enhancing Structure Properties of TiO_2 and Its Applications in Photodegradation and Hydrogen Evolution. *ACS Omega* **2022**, *6*, 30386–30400. [CrossRef]
31. El-Hakam, A.; Shorifi, T.A.L.; Salama, S.; Gamal, S.; El-Yazeed, W.S.A.; Ibrahim, A.A.; Ahmed, I. Application of nanostructured mesoporous silica/bismuth vanadate composite catalysts for the degradation of methylene blue and brilliant green. *J. Mater. Res. Technol.* **2022**, *18*, 1963–1976. [CrossRef]
32. Yan, X.; Jin, Z. Interface Engineering: NiAl-LDH in-situ derived NiP_2 quantum dots and Cu_3P nanoparticles ingeniously constructed p-n heterojunction for photocatalytic hydrogen evolution. *Chem. Eng. J.* **2020**, *420*, 2. [CrossRef]
33. Yan, X.; An, H.; Chen, Z.; Yang, G. Significantly enhanced charge transfer efficiency and surface reaction on NiP2/g-C3N4 heterojunction for photocatalytic hydrogen evolution. *Chin. J. Chem. Eng.* **2022**, *43*, 31–39. [CrossRef]
34. Zhang, Z.; Li, Q.; Qiao, X.; Hou, D.; Li, D. One-pot Hydrothermal Synthesis of Willow Branch-shaped MoS_2/CdS Heterojunctions for Photocatalytic H_2 Production Under Visible Light Irradiation. *Chin. J. Catal.* **2019**, *40*, 371–379. [CrossRef]
35. Zhang, K.; Feng, S.; Wang, J.; Azcatl, A.; Lu, N.; Addou, R.; Wan, N.; Zhou, C.; Lerach, J.; Bojan, V.; et al. Manganese doping of monolayer MoS_2: The substrate is critical. *Nano Lett.* **2015**, *15*, 6586–6591. [CrossRef] [PubMed]
36. Zhang, Y.; Liu, Y.; Ma, M.; Ren, X.; Liu, Z.; Du, G.; Asiri, A.M.; Sun, X. A Mn-doped Ni_2P nanosheet array: An efficient and durable hydrogen evolution reaction electrocatalyst in alkaline media. *Chem. Commun.* **2017**, *53*, 11048–11051. [CrossRef] [PubMed]
37. Bolara, S.; Shita, S.; Kumara, J.S.; Murmu, N.C.; Ganeshc, R.S.; Inokawa, H.; Kuila, T. Optimization of active surface area of flower like MoS_2 using V-doping towards enhanced hydrogen evolution reaction in acidic and basic medium. *Appl. Catal. B-Environ.* **2019**, *254*, 432–442. [CrossRef]
38. Bi, L.; Xu, D.; Zhang, L.; Lin, Y.; Wang, D.; Xie, T. Metal Ni-loaded g-C3N4 for enhanced photocatalytic H2 evolution activity: The change in surface band bending. *Phys. Chem. Chem. Phys.* **2015**, *17*, 29899–29905. [CrossRef]
39. Lu, Y.; Chu, D.; Zhu, M.; Du, Y.; Yang, P. Exfoliated carbon nitride nanosheets decorated with NiS as an efficient no-ble-metal-free visible-light-driven photocatalyst for hydrogen evolution. *Phys. Chem. Chem. Phys.* **2015**, *17*, 17355–17361. [CrossRef]
40. Bhunia, M.K.; Yamauchi, K.; Takanabe, K. Harvesting Solar Light with Crystalline Carbon Nitrides for Efficient Photocatalytic Hydrogen Evolution. *Angew. Chem. Int. Ed.* **2014**, *41*, 11001–11005. [CrossRef]
41. Zhao, H.; Sun, S.N.; Jiang, P.P.; Xu, Z.J. Graphitic C_3N_4 modified by Ni_2P cocatalyst: An efficient, robust and low cost photocatalyst for visible-light-driven H2 evolution from water. *Chem. Eng. J.* **2017**, *35*, 296–303. [CrossRef]
42. Wang, J.; Chen, J.; Wang, P.; Hou, J.; Wang, C.; Ao, Y. Robust photocatalytic hydrogen evolution over amorphous ruthenium phosphide quantum dots modified g-C_3N_4 nanosheet. *Appl. Catal. B-Environ.* **2018**, *239*, 578–585. [CrossRef]
43. Lin, Q.; Li, L.; Liang, S.; Liu, M.; Bi, J.; Wu, L. Efficient synthesis of monolayer carbon nitride 2D nanosheet with tunable concentration and enhanced visible-light photocatalytic activities. *Appl. Catal. B Environ.* **2015**, *163*, 135–142. [CrossRef]
44. Chen, Z.; Song, Y.; Cai, J.; Zheng, X.; Han, D.; Wu, Y.; Zang, Y.; Niu, S.; Liu, Y.; Zhu, J.; et al. Tailoring the d-band centers enables Co_4N nanosheets to be highly active for hydrogen evolution catalysis. *Angew. Chem. Int. Ed.* **2018**, *57*, 5076–5080. [CrossRef] [PubMed]
45. Yu, X.; Zhang, S.; Li, C.; Zhu, C.; Chen, Y.; Gao, P.; Qi, L.; Zhang, X. Hollow CoP nanopaticle/N-doped graphene hybrids as highly active and stable bifunctional catalysts for full water splitting. *Nanoscale* **2016**, *8*, 10902–10907. [CrossRef]
46. Jiang, P.; Liu, Q.; Sun, X.P. NiP_2 nanosheet arrays supported on carbon cloth: An efficient 3D hydrogen evolution cathode in both acidic and alkaline solutions. *Nanoscale* **2014**, *22*, 13440–13445. [CrossRef] [PubMed]
47. Dong, Y.; Kong, L.; Jiang, P.; Wang, G.; Zhao, N.; Zhang, H.; Tang, B. A general strategy to fabricate Ni_xP as highly efficient cocatalyst via photo-reduction deposition for hydrogen evolution. *ACS Sustain. Chem. Eng.* **2017**, *5*, 6845–6853. [CrossRef]
48. Xiao, L.; Tong, S.; Zhuo, W.; Zhang, K.; Peng, X.; Han, Y. Enhanced photocatalytic hydrogen evolution by loading $Cd_{0.5}Zn_{0.5}S$ QDs onto Ni_2P porous nanosheets. *Nanoscale Res. Lett.* **2018**, *13*, 31–40. [CrossRef]
49. Luo, Y.; Qin, J.; Yang, G.; Luo, S.; Zhao, Z.; Ma, M.C.J. N-Ni-S coordination sites of NiS/C_3N_4 formed by an electrochemical-pyrolysis strategy for boosting oxygen evolution reaction. *Chem. Eng. J.* **2021**, *410*, 128394. [CrossRef]